Mesh Parameterization by Minimizing the Synthesized Distortion Metric with the Coefficient-Optimizing Algorithm

Jingqi Yan, Xin Yang, Pengfei Shi, *Senior Member*, *IEEE*, and David Zhang, *Senior Member*, *IEEE*

Abstract—The parameterization of a 3D mesh into a planar domain requires a distortion metric and a minimizing process. Most previous work has sought to minimize the average area distortion, the average angle distortion, or a combination of these. Typical distortion metrics can reflect the overall performance of parameterizations but discount high local deformations. This affects the performance of postprocessing operations such as uniform remeshing and texture mapping. This paper introduces a new metric that synthesizes the average distortions and the variances of both the area deformations and the angle deformations over an entire mesh. Experiments show that, when compared with previous work, the use of synthesized distortion metric performs satisfactorily in terms of both the average area deformation and the average angle deformation; furthermore, the area and angle deformations are distributed more uniformly. This paper also develops a new iterative process for minimizing the synthesized distortion, the coefficient-optimizing algorithm. At each iteration, rather than updating the positions immediately after the local optimization, the coefficient-optimizing algorithm first update the coefficients for the linear convex combination and then globally updates the positions by solving the Laplace system. The high performance of the coefficient-optimizing algorithm has been demonstrated in many experiments.

Index Terms—Mesh parameterization, texture mapping, barycentric mapping, conformal mapping, harmonic mapping.

1 Introduction

Mesh parameterization addresses the problem of mapping a piecewise linear mesh surface into either a planar domain [6], [7], a spherical domain [10], [13], an octahedral domain [23], or a polygonal domain consisting of a base mesh [12], [17]. Mesh parameterization has many applications, including texture mapping [2], [13], [18], [19], [20], [21], [25], [27], remeshing [1], [3], [15], multiresolution representation [6], [12], [17], and geometric images [11]. This paper focuses on the planar parameterization or, as it is also known, surface flattening [2], [31]. Most recent works [4], [5], [20], [24], [25], [27], [28], [32] have focused on defining the distortion and showing how to minimize it.

The most commonly used distortion metric for an entire mesh is the area-weighted average norm [4], [25], [32]. The distortion metric for a single triangle, however, is widely different, whether that includes the area deformation [4], [5], [21], the angle deformation [14], [20], [22], the length deformation [21], [25], [27], or any combination of these [4], [5], [21], [27]. The average norm is able to reflect the overall distortion in a mesh parameterization, but discounts high local deformations. Several works [25], [28] have used the maximum norm, but it is not differentiable and cannot be quickly minimized. The most successful application of the maximum norm is to guarantee the distortion under a user-specified threshold by automatically partitioning and flattening the mesh [28]. To our knowledge, there little work has been done to date on the effective control of distortion variance. This is of interest because a smaller variance reflects a more balanced distortion distribution, which is desirable in many applications such as uniform remeshing, texture mapping, or geometric images.

In this paper, we introduce a new metric that synthesizes the average distortions and the variances of both the area deformations and the angle deformations over an entire mesh. This synthesized distortion metric is able to reflect not only the overall area and angle deformations, but also their distributions. Some textured results tested on the Mannequin model are shown in Fig. 1. The distributions of area deformation per triangle and of angle deformation per triangle are represented in Fig. 2. It can be seen that, when compared with the average geometric stretch [25], [32] and the combined energy [4], the use of the synthesized distortion metric produces comparable performance in terms of the average area deformation and the average angle deformation; furthermore, both the distribution of the area deformation per triangle and the distribution of the angle deformation per triangle in our results are much more uniform.

To minimize the synthesized distortion arising from an initial parameterization, we present a coefficient-optimizing algorithm, which is developed from the position-optimizing algorithm presented by Sander et al. [25]. At each loop, the position-optimizing algorithm updates the positions of all internal vertices in the parameter domain, computed by a linear search along a random direction. The position-optimizing algorithm is always effective but is very slow. A fast algorithm that iteratively diffuses the local geometric

- *J. Yan, X. Yang, and P. Shi are with the Institute of Image Processing and Pattern Recognition, Shanghai Jiao Tong University, Shanghai, China. E-mail: {jqyan, yangxin, pfshi}@sjtu.edu.cn.*
- *D. Zhang is with the Center for Multimedia Signal Processing, Department of Computing, Hong Kong Polytechnic University, Kowloon, Hong Kong. E-mail: csdzhang@comp.polyu.edu.hk.*

Manuscript received 6 Apr. 2004; revised 30 Apr. 2005; accepted 10 May 2005; published online 9 Nov. 2005.
For information on obtaining reprints of this article, please send e-mail to: tvcg@computer.org, and reference IEEECS Log Number TVCG-0035-0404.

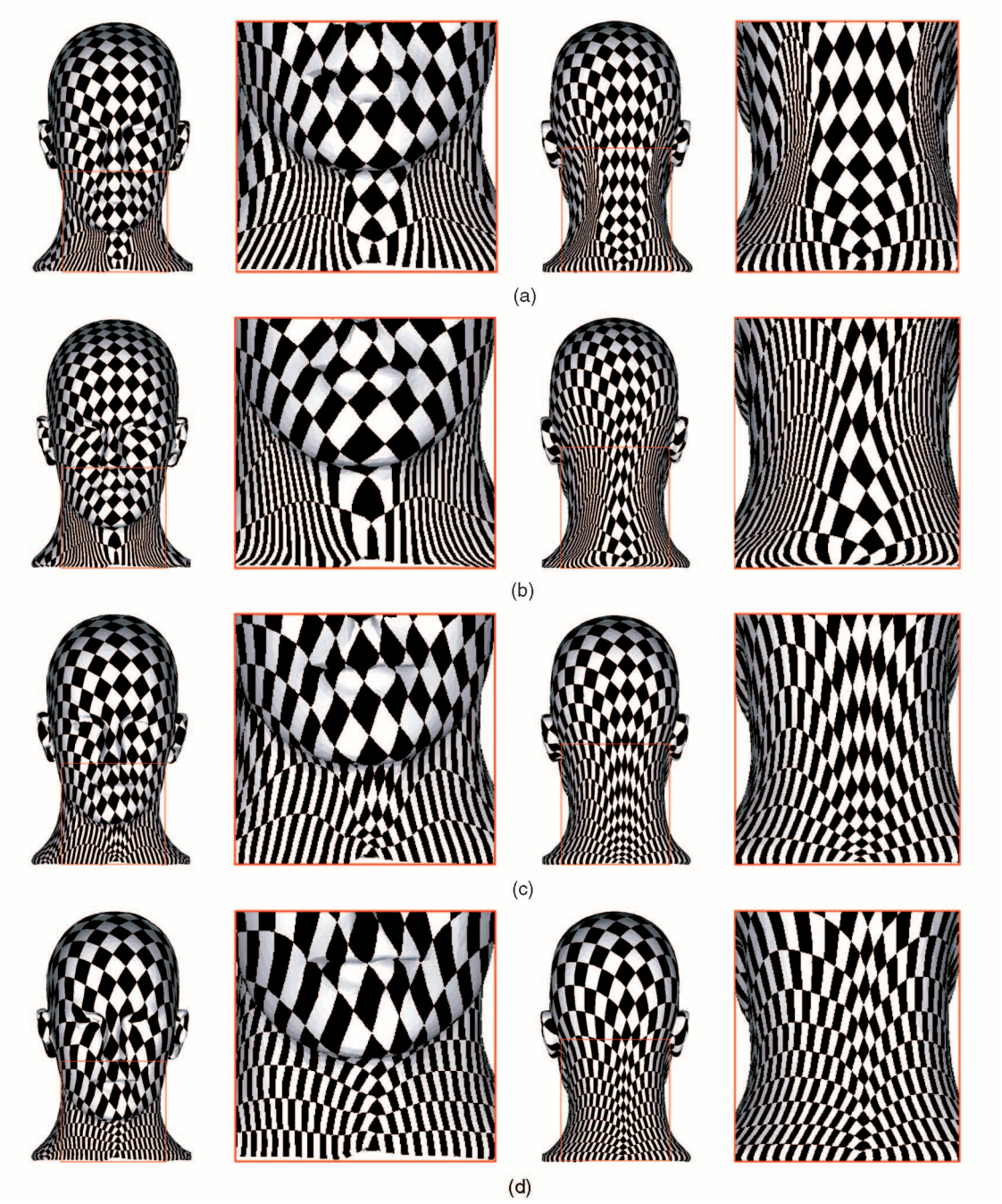

Fig. 1. The textured mannequin models parameterized by: (a) minmizing the average geometric stretch [25], (b) diffusing the average geometric stretch [32], (c) minimizing the combined energy [4], and (d) minimizing our synthesized distortion. For each parameterization, we map a chekerboard image with 128×128 pixels onto the mesh surface.

stretch was presented by Yoshizawa et al. [32]. For simplicity, we call this the coefficient-diffusing algorithm. The coefficient-diffusing algorithm can quickly lower the average geometric stretch, but is unstable for use in finer optimization. Unfortunately, it is not strong enough to directly minimize our synthesized distortion by diffusing the local synthesized distortion. Hence, we integrate the advantages of the position-optimizing algorithm and the coefficient-diffusing algorithm and present the coefficient-optimizing algorithm as a way of minimizing our synthesized distortion. This coefficient-optimizing algorithm computes the locally optimal position by searching linearly along a random direction, but, rather than updating the position immediately for all internal vertices, it converts the locally optimal position into the linear convex combination of its neighbors and updates the combination coefficients. The new positions of all internal vertices are thus globally determined by the Laplace operator [10]. Our experiments show that the coefficient-optimizing algorithm is computationally much faster than the position-optimizing algorithm [25]. Unlike the coefficient-diffusing algorithm [32], the coefficient-optimizing algorithm performs stably for finer optimization during the minimizing process.

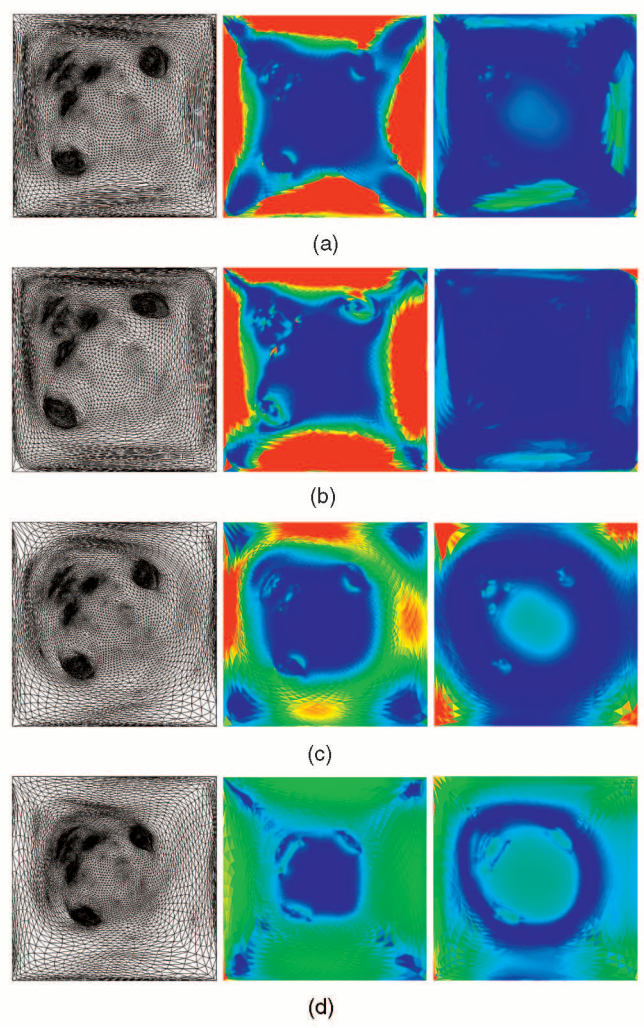

Fig. 2. The parameterization, per triangle angle deformation distribution and per triangle area deformation distribution tested on the mannequin model by: (a) mnimizing the average stretch [25], (b) diffusing the average stretch [32], (c) minimizing the combined energy [4], and (d) minimizing our synthesized distortion. In accordance with the per triangle angle (area) deformation, we assign the distortion range of $[2, 6.34+]$ ($[2, 6.63+]$) with colors from blue to red in all the distribution figures of angle (area) deformation. Statistical details of the maximum deformation, the average deformation, and the variance are summarized in Table 4 (Section 5).

The remainder of this paper is organized as follows: Section 2 reviews previous work. Section 3 introduces our new distortion metric. In Section 4, we describe the coefficient-optimizing algorithm. Section 5 offers some comparisons. Finally, Section 6 presents our conclusion.

2 Previous Work

A significant body of work on mesh parameterization has been published over the last 10 years. Most of the techniques described in this work sought to produce least-distorted parameterizations and varied only in the distortions they considered and the minimization processes that were used, broadly either linear or nonlinear.

The linear minimization methods ultimately convert the parameterization problem into a problem of computing a sparse linear system, which can be solved with the Conjugate Gradient methods [30]. The linear methods can be broadly subdivided, according to the distortions they addressed, into barycentric mapping, conformal mapping, and harmonic mapping methods.

Barycentric mapping was an early introduction of Tutte [29] and is used to make a straight line drawing of a planar graph. Within the barycentric mapping, any internal vertex is a linear convex combination of its neighbors in the parameterized domain. In Tutte's work, the weight coefficients for combination were evenly assigned. Floater [7] generalized barycentric mapping by considering the weight coefficients in terms of the local edge-length distortion and conformality, which was shape preserving in some sense. Levy and Mallet [19] took additional linear constraints into account and used the modified method for nondistorted texture mapping. More recently, Floater [8] further derived a generalization of barycentric mapping from the Mean Value Theorem for harmonic functions.

The purpose of conformal mapping is to minimize the distortion of the angles between the 3D mesh and its 2D parameterization. A number of authors have independently proposed discrete conformal parameterization (DCP) deriving the same linear condition for conformality either using Differential Geometry [22], harmonic maps [6], Finite Elements [18], or Cauchy-Riemann Equations [20].

Harmonic mapping was initially used by Eck et al. [6] for mesh multiresolution analysis and remeshing. Imagine a mesh composed of elastic, triangular rubber sheets sewn together along their edges. Stretch the boundary of the mesh over the boundary of a polygon according to the mapping. Using the elasticity theory, Eck et al. [6] interpreted the harmonic mapping by minimizing the total spring-like energy over this configuration of rubber sheets. Different spring-constant selection schemes [16] would produce very different results.

The linear methods are generally simple, intuitive, and easy to compute, but, in many applications, the total performance is not always acceptable. In particular, they are not effective in capturing highly frequent details. Many complex distortion metrics for improving the performance of mesh parameterization have been proposed, but these metrics usually cannot be minimized by computing a linear system.

Maillot et al. [21] minimize an edge-spring energy that preserves the edge length, but the best solution that computes a degree three polynomial might be to "fold" the map. To solve the problem of face folds, Maillot et al. also define an area-based energy using the difference of signed areas to penalize wrongly oriented triangles. The final energy is a linear combination of the edge-spring energy and the area-based energy. However, it is still not the case that this combined energy can guarantee the absence of face folds in the best solution [25]. Hormann and Greiner [14] have introduced a distortion metric with the Dirichlet energy per parameter area and proposed "most isometric parameterizations (MIPS)," which perfectly preserve angles. Sheffer and Sturler [26] minimize a pointwise criterion that is formulated in terms of the angles of the parameter triangles. Some nonlinear constraints have to be added to guarantee the validity of the solution. To reduce

the length distortion, they also present a second step that iteratively smoothes an overlay grid [27]. Sander et al. [25] minimize the average or maximum geometric stretch of a mapping to prevent undersampling. However, since they penalize only undersampling, some regions may exhibit high anisotropic stretch, consisting of slim triangles. Sorkine et al. [28] propose a maximum metric that compares the maximum stretch and the inverse of the minimum stretch, which penalizes both under and oversampling. Their functionality is not differentiable and is consequently hard to minimize. Instead, they use the maximum metric guaranteeing the distortion remains under a user-specified threshold by simultaneously cutting and flattening the mesh. Desbrun et al. [5] minimize a linear combination distortion of a discrete conformal energy and a discrete authalic energy, which can be converted into computing a linear system. However, the combined conformal and authalic energy remedies only local angle and area deformations. The performance of their algorithm is the same as that of Floater's shape preserving algorithm [7]. Recently, Degener et al. [4] extended the MIPS method for identifying parameterizations that mediate between angle and area deformations. The user can use a parameter to control the trade-off between the degree of angle and global area preservation.

In this paper, we propose a synthesized metric for measuring the distortion between the 3D mesh and its parameter version. Like the metric presented by Degener et al. [4], our synthesized metric takes into consideration both the average area deformation and the average angle deformation. Our synthesized metric also deals with variances, which reflect the distribution of the distortion of angle and area deformations.

3 The Synthesized Distortion Metric

Consider the case of a parameterization:

$$\phi : D \rightarrow M : (u, v) \in R^2 \rightarrow (x, y, z) \in R^3,$$

where D is a planar domain. At any point (u, v), the singular values Γ and γ of the 3×2 Jacobian matrix $J_\phi = [\, d\phi/du \quad d\phi/dv \,]$ represent the largest and smallest lengths obtained when mapping unit-length vectors from the domain D to the surface S, i.e., the largest and smallest local stretch over all directions in the domain [25]. In a triangular mesh, ϕ is piecewise linear and its Jacobian J_ϕ is constant over each triangle.

Based on the singular values Γ and γ of J_ϕ, Hormann and Greiner [14] derive a functional to measure the angle deformation X_i between a triangle T_i in 3D mesh and its 2D version:

$$\mathrm{X}_i = \frac{\Gamma_i}{\gamma_i} + \frac{\gamma_i}{\Gamma_i}.$$

Recently, Degener et al. [4] have developed a functional for measuring the area deformation Υ_i between them:

$$\Upsilon_i = \Gamma_i \gamma_i + \frac{1}{\Gamma_i \gamma_i}.$$

Therefore, we can obtain the maximum distortions, the average distortions, and the variances of both the angle and area deformations over the entire mesh $\{T_i\}_{i=1}^K$:

$$\begin{aligned}
\mathrm{X}_\infty &= \max(\mathrm{X}_i),\ i = 1, \cdots, K \\
\bar{\mathrm{X}} &= \mathrm{E}(\mathrm{X}_i) = \sum_{i=1}^{K} \rho_i \mathrm{X}_i, \\
\sigma_{\mathrm{X}}^2 &= \mathrm{E}((\mathrm{X}_i - \bar{\mathrm{X}})^2) = \sum_{i=1}^{K} \rho_i (\mathrm{X}_i - \bar{\mathrm{X}})^2, \\
\Upsilon_\infty &= \max(\Upsilon_i),\ i = 1, 2, \cdots, K \\
\bar{\Upsilon} &= \mathrm{E}(\Upsilon_i) = \textstyle\sum_{i=1}^{K} \rho_i \Upsilon_i, \\
\sigma_\Upsilon^2 &= \mathrm{E}((\Upsilon_i - \bar{\Upsilon})^2) = \sum_{i=1}^{K} \rho_i (\Upsilon_i - \bar{\Upsilon})^2,
\end{aligned}$$

where K is the number of triangles in the mesh; X_∞, $\bar{\mathrm{X}}$, and σ_{X}^2 denote the maximum distortion, the average distortion, and the variance of the angle deformations over the entire mesh; Υ_∞, $\bar{\Upsilon}$, and σ_Υ^2 denote the maximum distortion, the average distortion, and the variance of the area deformations over the entire mesh. The probability ρ_i is computed by the area ratio,

$$\rho_i = A(T_i) \Big/ \sum_{i=1}^{K} A(T_i),$$

where $A(T_i)$ is the area of triangle T_i in the 3D mesh. Note that Υ_∞, $\bar{\Upsilon}$, and σ_Υ^2 vary with the size of the parameter domain. To normalize them, without loss of generality, we first scale the parameter domain so that its area equals the surface area of the 3D mesh.

An ideal parameterization makes use of not only the smallest average distortions, but also the smallest variances of the angle and area deformations. Hence, we introduce a synthesized metric to jointly investigate them:

$$\eta = \bar{\mathrm{X}}^{1+\sigma_{\mathrm{X}}^2} \bar{\Upsilon}^{1+\sigma_\Upsilon^2}.$$

For convenience of computation, we can rewrite the synthesized distortion metric into the logarithmic format:

$$\eta_{\log} = (1 + \sigma_{\mathrm{X}}^2) \log_2 \bar{\mathrm{X}} + (1 + \sigma_\Upsilon^2) \log_2 \bar{\Upsilon}.$$

The synthesized distortion over the entire mesh can be minimized by iteratively reducing the local synthesized distortion over the neighborhood incident to each internal vertex. Since $\bar{\mathrm{X}} \geq 2$ and $\bar{\Upsilon} \geq 2$, a lower bound of $\eta_{\log}$ is 2 for any parameterization.

4 The Coefficient-Optimizing Algorithm

Here, we first introduce some notations. $\mathbf{x}_i = \{x_i, y_i, z_i\}$ and $\mathbf{u}_i = \{u_i, v_i\}$ denote the coordinates of a vertex V_i in the 3D mesh and its 2D version in the parameter domain, respectively. (i, j) represents the edge connecting V_i and V_j, and E denotes the set of all the edges in the mesh. $\mathbf{A}$, referred to as a Laplace operator [10], is an $n \times n$ matrix containing a_{ij}, where n is the number of internal vertices in the mesh. V_i^Δ and V_i^* denote the set of triangles and the set of vertices, respectively, incident to V_i.

Assume, by relabeling vertices if necessary, that $\{V_i\}_{i=1}^{n}$ are the internal vertices and $\{V_i\}_{i=n+1}^{N}$ are the boundary vertices in any counterclockwise sequence, where N is the number of all the vertices in the mesh. It is known [9] that each internal vertex V_i can be represented with the convex linear combination of its neighbors for a one-to-one parameterizetion, that is,

$$\mathbf{u}_i = \sum_{j=1,j\neq i}^{n} \lambda_{ij}\mathbf{u}_j + \sum_{j=n+1}^{N} \lambda_{ij}\mathbf{u}_j, \lambda_{ij}\begin{cases} = 0, & \text{if } (i,j) \notin E \\ > 0, & \text{if } (i,j) \in E \end{cases}, \text{ and}$$
$$\sum_{j=1,j\neq i}^{N} \lambda_{ij} = 1,$$

where λ_{ij}, $1 \le j \le N$ and $j \neq i$, are the coefficients for the convex linear combination; $\mathbf{u}_j$, $1 \le j \le n$, is the coordinates of one internal vertex V_j in the parameterization P; and $\mathbf{u}_j$, $n+1 \le j \le N$, is the coordinates of one boundary vertex that is pinned in the whole minimizing process. The representation above can be rewritten into the sparse matrix format: $\mathbf{A}(\mathbf{u}_1, \cdots, \mathbf{u}_n)^{\mathrm{T}} = (\mathbf{b}_1, \mathbf{b}_2)$, where $a_{ij} = 1$ if $i = j$ and, otherwise, $a_{ij} = -\lambda_{ij}$, $1 \le i, j \le n$;

$$\mathbf{b}_1 = \left(\sum_{j=n+1}^{N} \lambda_{1j}u_{\mathrm{j}}, \cdots, \sum_{j=n+1}^{N} \lambda_{nj}u_{\mathrm{j}} \right)^{\mathrm{T}}$$

and

$$\mathbf{b}_2 = \left(\sum_{j=n+1}^{N} \lambda_{1j}v_{\mathrm{j}}, \cdots, \sum_{j=n+1}^{N} \lambda_{nj}v_{\mathrm{j}} \right)^{\mathrm{T}}.$$

It can be easily divided into two linear systems and solved using the Conjugate Gradient methods.

Now, the coefficient-optimizing algorithm for mesh parameterization is given as follows:

Step 1: Given a threshold $\varepsilon > 0$ and an initial one-to-one parameterization P^0, the distortion over the entire mesh M corresponding to P^0 is $\eta_{\log}^0(M)$. Set the number of iterations and the current number of "redo" operators to be $q = 0$ and $r = 0$, respectively. Suppose the maximum number of continuous "redo" operators is $MaxR$ (in our experiments, $MaxR = 5$).

Step 2: For each internal vertex V_i with the parameterized coordinates $\mathbf{u}_i^q$ and the coefficients λ_{ij}^q, perform three operations:

Step 2.1: In the neighborhood V_i^{Δ}, fix its neighboring vertices and find a new position $\mathbf{u}'_i$ to make the local distortion $\eta_{\log}^q(V_i^{\Delta})$ minimal by searching the line along a randomly given direction [25].

Step 2.2: Compute the new combination [7]: $\mathbf{u}'_i = \lambda'_{i,d_1}\mathbf{u}^q_{i,d_1} + \lambda'_{i,d_2}\mathbf{u}^q_{i,d_2} + \cdots + \lambda'_{i,d_k}\mathbf{u}^q_{i,d_m}$, where m is the degree of V_i and $\mathbf{u}^q_{i,d_k}$, $1 \le k \le m$, are the coordinates of one neighboring vertex $V_{i,d_k} \in V_i^*$ in the parameterization P^q.

Step 2.3: Update. Note that we update the coefficients incident to V_i rather than the coordinate position. That is,

$$\lambda_{ij}^{q+1} = \begin{cases} \lambda'_{i,d_k}, & \text{if } j = d_k \\ \lambda_{ij}^q, & \text{otherwise.} \end{cases}$$

Step 3: Obtain the new Laplace operator [10], $\mathbf{A}^{q+1}$, and the right-hand vectors, $\mathbf{b}_1^{q+1}$ and $\mathbf{b}_2^{q+1}$ according to the new coefficients, λ_{ij}^{q+1}. Then, compute the new parameterization P^{q+1} with the new coordinates $\{\mathbf{u}_i^{q+1}\}_{i=1}^{n}$ by solving the 2D vector Laplace equation: $\mathbf{A}^{q+1}(\mathbf{u}_1, \cdots, \mathbf{u}_n)^{\mathrm{T}} = (\mathbf{b}_1^{q+1}, \mathbf{b}_2^{q+1})$.

Step 4: Compute $\eta_{\log}^{q+1}(M)$, the new distortion over the entire mesh M corresponding to P^{q+1}, and get the difference, $\Delta^q = \eta_{\log}^q(M) - \eta_{\log}^{q+1}(M)$. If $\Delta^q \ge \varepsilon$, then $q = q+1$, $r = 0$ and go to Step 2. If $0 \le \Delta^q < \varepsilon$ and $r < MaxR$, then $q = q+1$, $r = r+1$ and go to Step 2. If $0 \le \Delta^q < \varepsilon$ and $r \ge MaxR$, then stop the iterative process. If $\Delta^q < 0$ and $r < MaxR$, then $P^{q+1} = P^q$, $q = q+1$, $r = r+1$ and go to Step 2. If $\Delta^q < 0$ and $r \ge MaxR$, then $P^{q+1} = P^q$, $q = q+1$ and stop the iterative process.

Note that the coefficient-optimizing algorithm can also be used to minimize the average stretch [25] by replacing $\eta_{\log}(M)$ with $L_2(M)$ and to minimize the combined energy [4] by replacing $\eta_{\log}(M)$ with $E(\phi)$. We think it can be generalized to minimize other nonlinear distortions, except the maximum distortion.

It is guaranteed by the coefficient-optimizing algorithm that the parameterization holds one-to-one if the boundary is mapped to a convex shape since the local optimizations are restricted to the kernel of the neighborhoods and the coefficients transferred to the Laplace solver are positive.

There is, however, no theoretical guarantee that the coefficient-optimizing algorithm will reduce the global distortion after each iteration since the local attributes are used for the global optimization. However, it is rarely the case that, after one iteration, there is no improvement. Even if it does occur, the random search scheme can handle it effectively using the "redo" operator. That is, if the distortion after the current iteration is larger than that after the previous iteration, we reuse the data from the previous iteration to perform the next iteration.

In order to find the best possible solution, we also employ a termination condition based on multiple confirmations. That is, the whole iterative process terminates if and only if all of several continuous times of iterations fail to reduce the distortion or if their reductions are smaller than the predefined threshold, ε. A termination condition based on multiple confirmations also assists the position-optimizing algorithm. This is because the random search scheme is not always highly efficient; consequently, if the termination condition depended on just one confirmation, the minimizing process may stop too early.

5 Experiments and Comparisons

In this section, we will discuss and compare several tested models topologically equivalent to a disk, as shown in Fig. 3, the different distortion metrics, and the minimizing methods used for mesh parameterization. The unit square is used as the parameter domain and the boundary vertices of each model are fixed on the boundary of the square.

All the experiments are performed on an HP Workstation XW6000 with a Xeon 2.8GHZ processor and 1GB DDR266 RAM. To solve a system of linear equation $\mathbf{Ax} = \mathbf{b}$, we use Bi-CGSTAB [30] with the maximum number of iterations equal to 10^4 and the relative error $\|\mathbf{Ax} - \mathbf{b}\|/\|\mathbf{b}\|$ is set to 10^{-5}. The interior linear search method that is used for local position optimization in the coefficient-optimizing algorithm is similar to that used for the position-optimizing algorithm

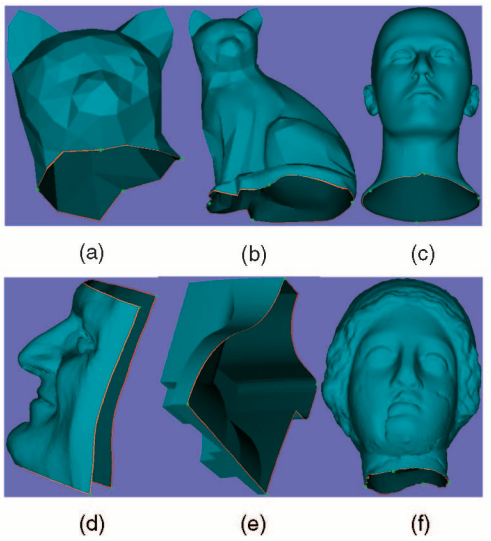

Fig. 3. The models tested in our experiments, their boundaries (red), and the pinned corners (green): (a) Cathead (#V = 110, #T = 206, A = 0.2165), (b) Cat (#V = 4,539, #T = 5,976, A = 9.6217), (c) Mannequin (#V = 6,768, #T = 13,471, A = 16.3168), (d) Fran (#V = 4,104, #T = 7,787, A = 3.3239), (e) Fandisk (#V = 5,051, #T = 9,926, A = 4.5831), and (f) Venushead (#V = 13,876, #T = 27,614, A=56.2422). Here, #V is the number of vertices, #T is the number of triangles, and A is the surface area.

[25]. The convergent threshold ε for the iterative minimizing process is set to 10^{-4}.

5.1 The Influence of the Initial Parameterization

To minimize the nonlinear distortion, we start from an initial one-to-one parameterization. Commonly, an initial parameterization will be produced using a linear method. To show the influence of the different initials on the optimized results, we perform the experiments that use methods from Kent et al., including uniform [16] which is similar to Tutte's [29] and proportional to the edge length [16], Eck et al. [6], Floater including shape preserving [7] and mean value [8], and Pinkall and Polthier [22]. On all the tested models in our experiments, the barycentric mapping methods [7], [8], [16], [29] always produce one-to-one parameterization, while the conformal mapping method [22] and the harmonic mapping method [6] produce one-to-one parameterization only on the Cathead and Fandisk models.

Table 1 summarizes the optimized results from the different initials on the Cathead and Fandisk models. One can see that the initial parameterization will not significantly affect the quality of the minimization of the final results obtained by our coefficient-optimizing algorithm, although the algorithm ends at a different local optimal.

As Yoshizawa et al. [32] used Floater's shape preserving algorithm [7] for their initial parameterization, for the purpose of comparison, we begin the following experiments in the same way.

5.2 Performance Analysis: Minimizing Processes

This section compares the performance of three algorithms in mesh parameterization minimization processes. The algorithms are the position-optimizing algorithm [25], the coefficient-diffusing algorithm [32], and the coefficient-optimizing algorithm.

TABLE 1
Influence on the Optimized Results of Different Initial Parameterizations, Tested on the Cathead and Fandisk Models

Algorithms for Initial Parameterization	Initial Parameterization					After optimizing η_{log}				
	$\overline{X}$	σ_X^2	$\overline{Y}$	σ_Y^2	η_{log}	$\overline{X}$	σ_X^2	$\overline{Y}$	σ_Y^2	η_{log}
The Cathead Model										
Uniform [29,16]	2.54	0.52	6.80	44.09	126.79	2.70	0.24	2.35	0.12	3.15
Proportional [16]	2.36	0.23	7.20	70.31	204.66	2.71	0.24	2.39	0.12	3.18
Harmonic [6]	2.25	0.14	5.65	59.88	153.46	2.64	0.21	2.35	0.11	3.07
Conformal [22]	2.25	0.14	5.65	59.88	153.46	2.63	0.21	2.37	0.11	3.07
Shape preserving [7]	2.30	0.18	5.27	26.58	67.53	2.63	0.20	2.36	0.11	3.06
Mean Value [8]	2.42	0.31	5.43	39.59	100.85	2.65	0.19	2.37	0.11	3.06
The Fandisk Model										
Uniform [29,16]	2.40	0.15	3.30	20.16	37.87	2.25	0.028	2.10	0.014	2.29
Proportional [16]	2.29	0.085	3.03	10.46	19.62	2.25	0.029	2.10	0.014	2.29
Harmonic [6]	2.13	0.024	2.59	2.21	5.53	2.24	0.029	2.10	0.015	2.29
Conformal [22]	2.13	0.024	2.59	2.21	5.53	2.24	0.030	2.10	0.015	2.29
Shape preserving [7]	2.18	0.030	2.72	3.40	7.53	2.24	0.029	2.10	0.015	2.29
Mean Value [8]	2.33	0.11	2.99	7.73	15.14	2.25	0.029	2.10	0.015	2.29

5.2.1 Processes for Minimizing the Average Geometric Stretch

Table 2 summarizes the running time and the results for minimizing the average stretch L_2 [25] using all three algorithms.

Both the coefficient-diffusing algorithm and the coefficient-optimizing algorithm are much faster than the position-optimizing algorithm. The coefficient-diffusing and coefficient-optimizing algorithms require many fewer iterations than the position-optimizing algorithm (tens of iterations versus hundreds, even up to thousands of iterations). As a result, even though they require longer for each single iteration, the coefficient-diffusing and coefficient-optimizing algorithms are quite efficient. Note that, on the Cat model, the results using the position-optimizing algorithm are still far from optimal, even when the algorithm satisfies the convergent condition (that is, the improvements among the continuous five iterations are less than 10^{-4}) after 2,000 iterations.

Fig. 4 illustrates in detail the process for minimizing the L_2 stretch on the Mannequin model using these three algorithms. The position-optimizing algorithm is very slow; the coefficient-diffusing algorithm is the most efficient for

TABLE 2
Results of Minimizing the Average Stretch Using Different Optimizing Algorithms

Models	Pos. Opt. [25]			Coeff. Diff. [32]			Coeff. Opt.		
	L_2	#	Time	L_2	#	Time	L_2	#	Time
Cathead	1.23	192	2s	1.28	8	0.06s	1.22	25	0.4s
Cat	5.62	2000	12m	1.45	4	5s	1.32	160	4m
Fandisk	1.12	410	4m	1.13	2	2.5s	1.09	15	23s
Fran	1.04	57	33s	1.10	1	0.7s	1.03	18	20s
Mannequin	1.52	4000	1h	1.41	4	10s	1.32	71	3m
Venushead	1.42	5263	3h	1.34	3	36s	1.25	90	15m

#= *the number of iterations, s= second(s), m= minute(s), h= hour(s).*

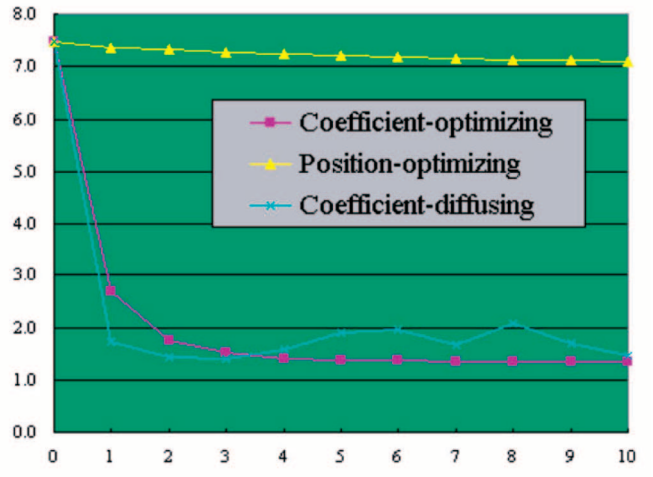

Fig. 4. The detailed process for minimizing the average geometric stretch using different algorithms on the Mannequin model. Here, we have the coefficient-diffusing algorithm perform 10 iterations.

producing a low-L_2-stretch parameterization, but it is unstable for finer optimization; the performance of the coefficient-optimizing algorithm is between the two: It is much faster than the position-optimizer and produces a more stable finer optimization than the coefficient-diffuser. The coefficient-optimizing algorithm thus always produces the best results in terms of the L_2 metric (see Table 2).

5.2.2 Processes for Minimizing the Synthesized Distortion

Table 3 shows the running time and the results for minimizing the synthesized distortion. On most of the models tested in our experiments, the coefficient-diffusing algorithm performs poorly at directly minimizing the synthesized distortion $\eta_{\log}$ by diffusing the local synthesized distortions. We think the effectiveness of the coefficient-diffusing algorithm depends on the "fluctuations" among the local distortions incident to all the internal vertices. Employing the $\eta_{\log}$ metric smooths fluctuations in the local distortions and, as a result, the coefficient-diffusing algorithm is less effective in directly minimizing the $\eta_{\log}$ distortion.

Generally, both the coefficient-optimizing algorithm and the position-optimizing algorithm are strong to directly minimize the synthesized distortion; however, as shown in Table 3, the coefficient-optimizer minimizes the synthesized distortion more effectively and faster.

TABLE 3
Results of Minimizing the Synthesized Distortion Using Different Optimizing Algorithms

Models	Pos. Opt. [25]			Coeff. Diff. [32]			Coeff. Opt.		
	$\eta_{\log}$	#	Time	$\eta_{\log}$	#	Time	$\eta_{\log}$	#	Time
Cathead	3.07	224	3s	12.41	1	<1s	3.06	22	<1s
Cat	4.92	1367	19m	3986.84	3	5s	3.69	12	18s
Fandisk	2.33	560	7m	3.07	2	3s	2.29	16	26s
Fran	2.10	91	1m	2.57	1	<1s	2.10	22	23s
Mannequin	40.03	1414	30m	7933.54	1	3s	4.20	39	2m
Venushead	5.11	7209	3.7h	960.56	1	12s	4.19	37	6m

#= *the number of iterations, s= second(s), m= minute(s), h= hour(s).*

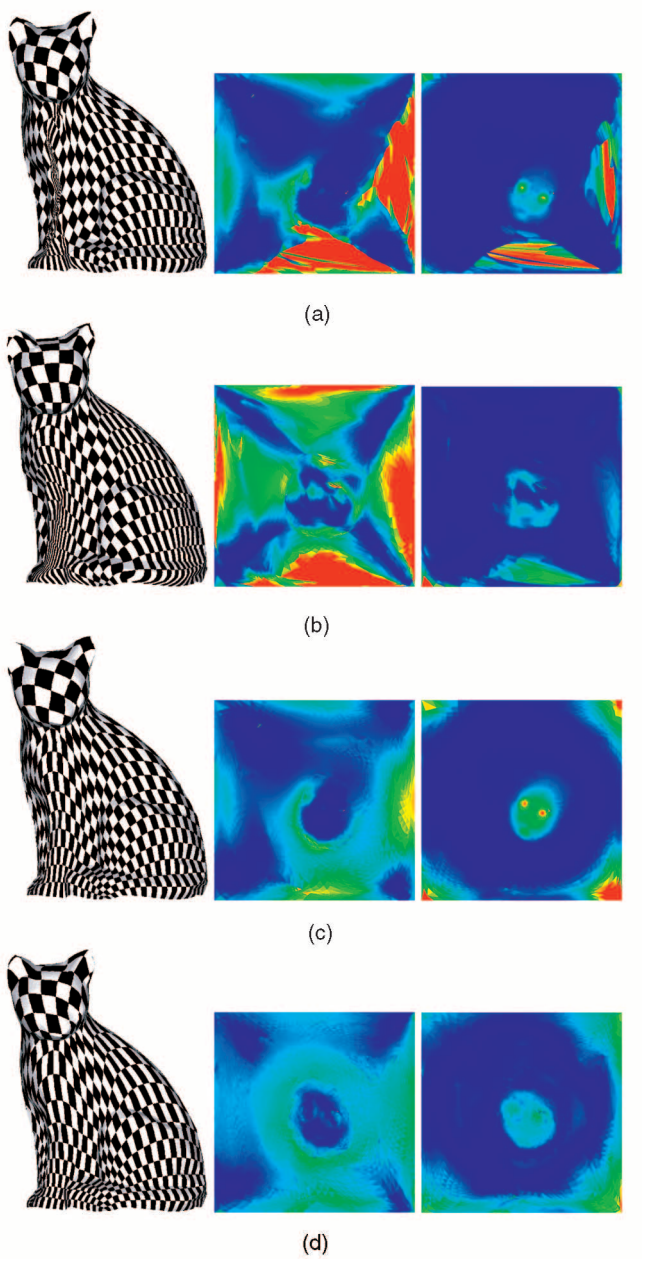

Fig. 5. The textured model, per triangle angle deformation distribution, and per triangle area deformation distribution tested on the Cat model by: (a) minimizing the average stretch [25], (b) diffusing the average stretch [32], (c) minimizing the combined energy [4], and (d) minimizing our synthesized distortion. In accordance with the per triangle angle (area) deformation, we assign the distortion rans of $[2, 8.68+]$ ($[2, 6.24+]$) with colors from blue to red in all of the distribution figures of angle (area) deformation. Statistical details of the maximum deformation, the average deformation, and the variance are summarized in Table 4.

5.3 Comparisons of the Distortion Metrics

Here, we will discuss the distortion metrics through the visualized and quantitative analyses in the context of one of the main applications of mesh parameterization, texture mapping, in which, for each parameterization, a 128×128 checkerboard image is mapped onto the mesh surface.

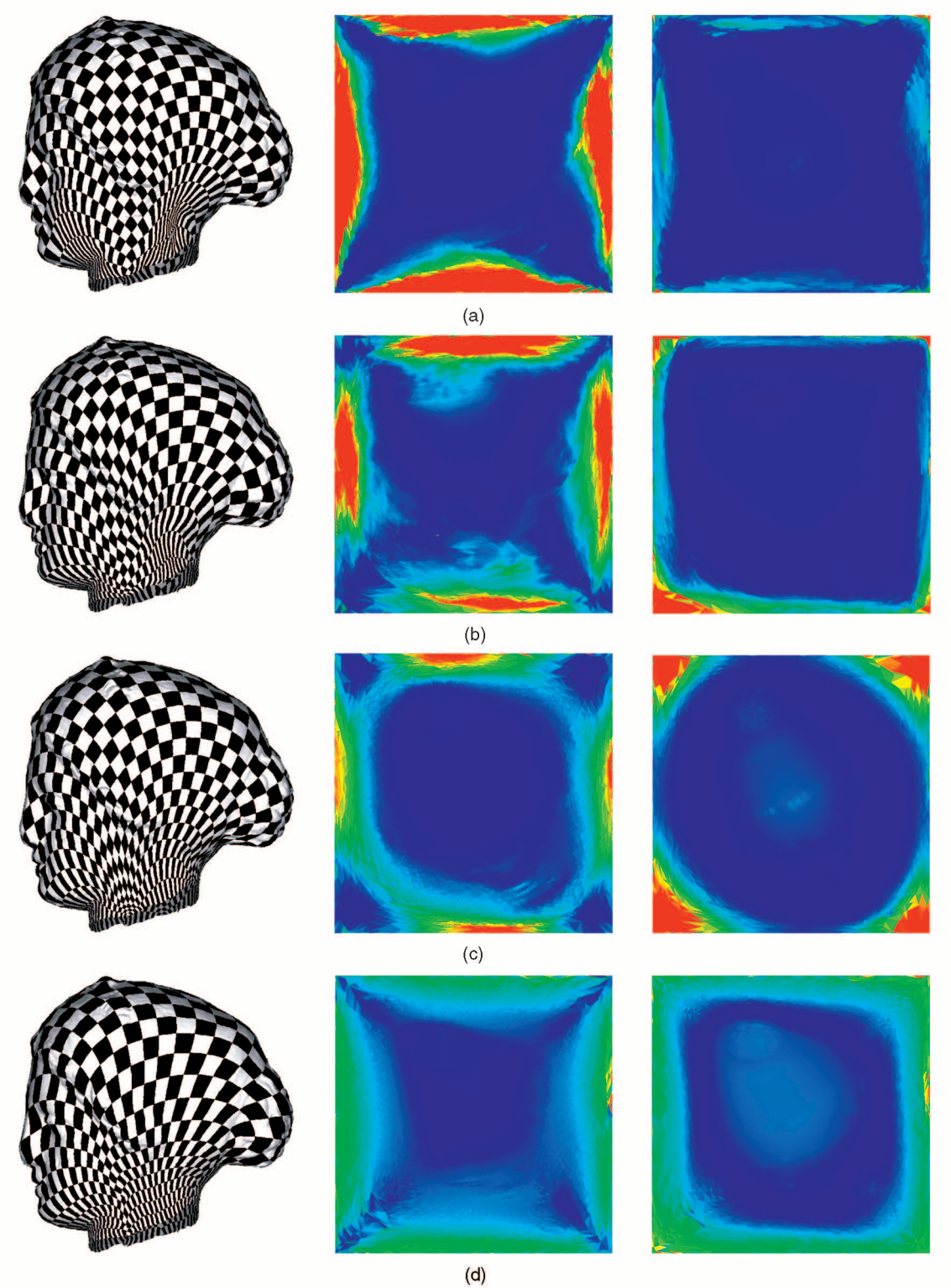

Fig. 6. The textured model, per triangle angle deformation distribution, and per triangle area deformation distribution tested on the Venushead model by: (a) minimizing the average stretch [25], (b) diffusing the average stretch [32], (c) minimizing the combined energy [4], and (d) minimizing our synthesized distortion. In accordance with the per triangle angle (area) deformation, we assign the distortion range of $[2, 10+]$ ($[2, 10+]$) with colors from blue to red in all of the distribution figures of angle (area) deformation. Statistical details of the maximum deformation, the average deformation, and the variance are summarized in Table 4.

In the following experiments, we use the coefficient-optimizing algorithm to minimize the L_2 stretch [25], the combined energy $E(\phi)$ [4], and the synthesized distortion $\eta_{\log}$, and use the coefficient-diffusing algorithm [32] to produce $\text{low-}L_2\text{-stretch}$ results.

Fig. 1 shows the textured Mannequin models. Fig. 2 shows the distributions of angle deformations and of area

TABLE 4
Quantitative Analyses of the Parameterized Results Using Different Distortion Metrics

Models	Goals	Angle related			Area related			$\eta_{\log}$
		X_∞	$\overline{X}$	σ_X^2	Y_∞	$\overline{Y}$	σ_Y^2	
Cathead	G0	4.50	2.30	0.18	35.09	5.27	26.58	67.53
	G1	6.14	2.83	0.91	3.48	2.16	0.041	4.02
	G2	7.15	3.16	1.33	4.76	2.12	0.062	5.02
	G3	5.19	2.59	0.42	6.24	2.29	0.24	3.43
	G4	4.67	2.63	0.20	4.90	2.36	0.11	3.06
Cat	G0	32.21	2.24	0.072	4264.17	51.59	27144.80	154436.11
	G1	146.82	3.75	44.17	14.42	2.23	0.29	87.58
	G2	79.24	4.16	6.28	11.14	2.19	0.094	16.19
	G3	28.74	3.00	0.81	12.67	2.39	0.44	4.70
	G4	8.68	3.25	0.33	6.24	2.36	0.15	3.69
Fandisk	G0	4.03	2.18	0.030	27.87	2.72	3.40	7.53
	G1	4.49	2.29	0.10	4.29	2.05	0.0095	2.36
	G2	4.66	2.38	0.15	4.57	2.06	0.014	2.50
	G3	3.89	2.22	0.063	4.65	2.09	0.025	2.32
	G4	2.98	2.24	0.029	3.10	2.10	0.015	2.29
Fran	G0	172.76	2.08	0.20	180.59	2.08	0.23	2.57
	G1	35.27	2.10	0.012	36.85	2.01	0.0049	2.10
	G2	172.76	2.08	0.20	180.59	2.08	0.23	2.57
	G3	44.82	2.09	0.010	46.85	2.03	0.011	2.10
	G4	50.39	2.09	0.011	52.70	2.02	0.010	2.10
Mannequin	G0	22.82	2.33	0.094	16482.80	47.24	4723.52	26279.20
	G1	35.37	3.69	14.67	7.91	2.28	0.11	30.82
	G2	193.38	4.42	23.45	24.34	2.17	0.10	53.65
	G3	9.80	3.00	1.59	23.25	2.55	0.41	6.02
	G4	6.34	2.86	0.46	6.63	2.98	0.26	4.20
Venushead	G0	81.04	2.08	0.096	685.28	17.94	229.32	960.56
	G1	89.49	3.29	12.03	10.83	2.23	0.11	23.67
	G2	247.69	3.32	5.18	49.86	2.26	0.37	12.30
	G3	49.54	2.73	1.62	44.74	2.48	0.81	6.16
	G4	13.94	2.68	0.47	14.41	2.81	0.40	4.19

G0 denotes the initial parameterization using Floater's Shaper preserving algorithm [7], G1 stands for minimizing the average geometric stretch [25], G2 stands for diffusing the average geometric stretch [32], G3 stands for minimizing the combined energy [4], and G4 stands for minimizing our synthesized distortion.

deformations in the parameter domain corresponding to the Mannequin model. Observing the "neck" region on the Mannequin model, the results obtained by minimizing/diffusing the L_2 stretch or the $E(\phi)$ energy have much larger area or angle deformations than the result obtained by minimizing our $\eta_{\log}$ distortion. Fig. 5 and Fig. 6 show the results of tests on the Cat model and the Venushead model. It is noticeable that the "paw" region on the Cat model and the "neck" region on the Venushead model in the results obtained by minimizing/diffusing the L_2 stretch or the $E(\phi)$ energy have larger area or angle deformations than the corresponding regions in the results obtained by minimzing our $\eta_{\log}$ distortion.

The quantitative results obtained by minimizing/diffusing the L_2 stretch [25], [32], the $E(\phi)$ energy [4], or our $\eta_{\log}$ distortion are summarized in Table 4.

Both visual and numerical comparisons show that the L_2 stretch is more sensitive to the area deformation than to the angle deformation. Minimizing/diffusing the L_2 stretch can perfectly preserve the triangle area at the cost of the triangle conformality. While the $E(\phi)$ energy can balance the average area deformation and the average angle deformation, it leaves some regions with very large area or angle deformations. Compared with these distortion metrics, our $\eta_{\log}$ distortion metric can reflect not only the average area deformation and the average angle deformation, but also the area and angle deformation distributions.

6 Conclusion

This paper has studied the problem of planar parameterization for 3D surface meshes, focusing on the distortion metric and the minimizing process, and presents a new distortion metric which synthesizes the average distortion and the distortion distribution of both the area deformation and the angle deformation. Experiments involving both quantitative analyses and practical texture mapping applications show that, when compared with previous work, our synthesized distortion metric performs satisfactorily in terms of both the average area deformation and the average angle deformation. Furthermore, the area and angle deformations are distributed more uniformly among all the triangles in the mesh.

This paper also proposes a novel coefficient-optimizing algorithm for minimizing synthesized distortion. This algorithm integrates the advantages of the position-optimizing algorithm and of the coefficient-diffusing algorithm. In experiments, the coefficient-optimizing algorithm is computationally much faster than the position-optimizing algorithm. Compared with the coefficient-diffusing algorithm, the coefficient-optimizing algorithm is slower, but more effectively seeks approximately optimal solutions, an important quality, especially for minimizing synthesized distortion.

Acknowledgments

The authors would like to thank all those who have contributed to this work by providing their data, results, and comments. This work was partly supported by UGC/CERG Hong Kong Government, Central Fund of The Hong Kong Polytechnic University, the National Natural Science Foundation of China (No. 60402020, No. 69931010, No. 60273047), and the National Basic Research Program (973) of China (No. 2003CB716100).

References

[1] P. Alliez, M. Meyer, and M. Desbrun, "Interactive Geomety Remeshing," *Proc. ACM SIGGRAPH 2002,* pp. 347-354, 2002.
[2] C. Bennis, J.-M. Vézien, G. Iglésias, and A. Gagalowicz, "Piecewise Surface Flattening for Non-Distorted Texture Mapping," *Computer Graphics,* vol. 25, no. 4, pp. 237-246, July 1991.
[3] M. Botsch, C. Rössl, and L. Kobbelt, "Feature Sensitive Sampling for Interactive Remeshing," *Proc. Vision, Modeling, and Visualization 2000,* pp. 129-136, 2000.
[4] P. Degener, J. Meseth, and R. Klein, "An Adaptable Surface Parameterization Method," *Proc. 12th Int'l Meshing Roundtable,* pp. 227-237, 2003.
[5] M. Desbrun, M. Meyer, and P. Alliez, "Intrinsic Parametrizations of Surface Meshes," *Computer Graphics Forum,* vol. 21, no. 3, pp. 209-218, 2002.
[6] M. Eck, T. DeRose, T. Duchamp, H. Hoppe, M. Lounsbery, and W. Stuetzle, "Multiresolution Analysis of Arbitrary Meshes," *Proc. ACM SIGGRAPH '95,* pp. 173-182, Aug. 1995.

[7] M.S. Floater, "Parametrization and Smooth Approximation of Surface Triangulations," *Computer Aided Geometric Design,* vol. 14, no. 3, pp. 231-250, 1997.
[8] M.S. Floater, "Mean Value Coordinates," *Computer Aided Geometric Design,* vol. 20, no. 1, pp. 19-27, 2003.
[9] M.S. Floater and C. Gotsman, "How to Morph Tilings Injectively," *J. Computational and Applied Math.,* vol. 101, pp. 117-129, 1999.
[10] C. Gotsman, X. Gu, and A. Sheffer, "Fundamentals of Spherical Parameterization for 3D Meshes," *ACM Trans. Graphics,* vol. 22, no. 3, pp. 358-363, July 2003.
[11] X. Gu, S. Gortler, and H. Hoppe, "Geometry Images," *Proc. ACM SIGGRAPH 2002,* pp. 355-361, 2002.
[12] I. Guskov, K. Vidimce, W. Sweldens, and P. Schröder, "Normal Meshes," *Proc. ACM SIGGRAPH 2000,* pp. 95-102, 2000.
[13] S. Haker, S. Angenent, A. Tannenbaum, R. Kikinis, G. Sapiro, and M. Halle, "Conformal Surface Parameterization for Texture Mapping," *IEEE Trans. Visualization and Computer Graphics,* vol. 6, no. 2, pp. 181-189, Apr.-June 2000.
[14] K. Hormann and G. Greiner, "MIPS: An Efficient Global Parameterization Method," *Curve and Surface Design: Saint-Malo 1999,* P.-J. Laurent, P. Sablonnière, and L.L. Schumaker, eds., pp. 153-162, Nashville Tenn.: Vanderbilt Univ. Press, 2000.
[15] K. Hormann, U. Labsik, and G. Greiner, "Remeshing Triangulated Surfaces with Optimal Parameterizations," *Computer-Aided Design,* vol. 33, no. 11, pp. 779-788, 2001.
[16] J.R. Kent, W.E. Carlson, and R.E. Parent, "Shape Transformation for Polyhedral Objects," *Proc. ACM SIGGRAPH '92,* pp. 47-54, July 1992.
[17] A. Lee, W. Sweldens, P. Schröder, L. Cowsar, and D. Dobkin, "MAPS: Multiresolution Adaptive Parameterization of Surfaces," *Proc. ACM SIGGRAPH '98,* pp. 95-104, 1998.
[18] B. Lévy, "Constrained Texture Mapping for Polygonal Meshes," *Proc. ACM SIGGRAPH 2001,* pp. 417-424, Aug. 2001.
[19] B. Lévy and J.L. Mallet, "Non-Distorted Texture Mapping for Sheared Triangulated Meshes," *Proc. ACM SIGGRAPH '98,* pp. 343-352, 1998.
[20] B. Lévy, S. Petitjean, N. Ray, and J. Maillot, "Least Squares Conformal Maps for Automatic Texture Atlas Generation," *Proc. ACM SIGGRAPH 2002,* pp. 362-371, 2002.
[21] J. Maillot, H. Yahia, and A. Verroust, "Interactive Texture Mapping," *Proc. ACM SIGGRAPH '93,* pp. 27-34, 1993.
[22] U. Pinkall and K. Polthier, "Computing Discrete Minimal Surfaces and Their Conjugates," *Experimental Math.,* vol. 2, no. 1, pp. 15-36, 1993.
[23] E. Praun and H. Hoppe, "Spherical Parameterization and Remeshing," *ACM Trans. Graphics,* vol. 22, no. 3, pp. 340-349, July 2003.
[24] P. Sander, S. Gortler, J. Snyder, and H. Hoppe, "Signal Specialized Parametrization," *Proc. Eurographics Workshop Rendering 2002,* pp. 87-100, 2002.
[25] P. Sander, J. Snyder, S. Gortler, and H. Hoppe, "Texture Mapping Progressive Meshes," *Proc. ACM SIGGRAPH 2001,* pp. 409-416, 2001.
[26] A. Sheffer and E. Sturler, "Parameterization of Faceted Surfaces for Meshing Using Angle-Based Flattening," *Eng. with Computers,* vol. 17, no. 3, pp. 326-337, 2001.
[27] A. Sheffer and E. Sturler, "Smoothing an Overlay Grid to Minimize Linear Distortion in Texture Mapping," *ACM Trans. Graphics,* vol. 21, no. 4, pp. 874-890, Oct. 2002.
[28] O. Sorkine, D. Cohen-Or, R. Goldenthal, and D. Lischinski, "Bounded-Distortion Piecewise Mesh Parameterization," *Proc. IEEE Visualization 2002,* pp. 355-362, 2002.
[29] W.T. Tutte, "How to Draw a Graph," *Proc. London Math Soc.,* vol. 13, pp. 743-768, 1963.
[30] H.A. VanderVorst, "Bi-CGSTAB: A Fast and Smoothly Converging Variant of Bi-CG for the Solution of Nonsymmetric Linear Systems," *SIAMsci,* vol. 13, pp. 631-644, 1992.
[31] C.L. Wang, S.F. Smith, and M.F. Yuen, "Surface Flattening Based on Energy Model," *Computer-Aided Design,* vol. 34, no. 11, pp. 823-833, 2002.
[32] S. Yoshizawa, A. Belyaev, and H.-P. Seidel, "A Fast and Simple Stretch-Minimizing Mesh Parameterization," *Proc. Shape Modeling and Applications,* pp. 200-208, June 2004.

Jingqi Yan received the BS degree (1996) in automatic control and the MS (1999) and PhD (2002) degrees in pattern recognition and intelligent systems from Shanghai Jiao Tong University, Shanghai, China. He is currently a researcher in the Institute of Image Processing and Pattern Recognition at Shanghai Jiao Tong University. His interests include geometric modeling, computer graphics, biometrics, scientific visualization, and image processing.

Xin Yang holds the M.S degree in control engineering from Northwestern Polytechnic University, Xi'an, China in 1982 and the Doctor of Applied Science degree in electronic engineering from the Free University of Brussels (ETRO/VUB) in 1995. Since 1997, he has been with the Institute of Image Processing and Pattern Recognition, Shanghai Jiao Tong University, Shanghai, China. His current research activities are in the area of medical image analysis and partial differential equations in image procession. Dr. Yang is the author of more than 70 papers in journal and refereed conference proceedings.

Pengfei Shi received the Bachelor's and Master's degrees in electrical engineering from Shanghai Jiao Tong University (SJTU), Shanghai, China, in 1962 and 1965, respectively. In 1980, he joined the Institute of Image Processing and Pattern Recognition (IPPR), SJTU. During the past 23 years, he worked in the area of image analysis, pattern recognition, and visualization. He has published more than 80 papers. He is currently the director of the Institute of IPPR at SJTU and a professor of pattern recognition and intelligent systems on the Faculty of Electronic and Information Engineering. He is a senior member of the IEEE.

David Zhang graduated in computer science from Peking University in 1974 and received the MSc and PhD degrees in computer science and engineering from the Harbin Institute of Technology (HIT) in 1983 and 1985, respectively. From 1986 to 1988, he was a postdoctoral fellow at Tsinghua University and became an associate professor at the Academia Sinica, Beijing, China. He received his second PhD degree in electrical and computer engineering from the University of Waterloo, Ontario, Canada, in 1994. Currently, he is a professor at the Hong Kong Polytechnic University. He is the founder and director of two Biometrics Technology Centers supported by the Government of the Hong Kong SAR (UGC/CRC) and the National Nature Scientific Foundation (NSFC) of China, respectively. He is also the founder and editor-in-chief of the *International Journal of Image and Graphics* (*IJIG*), book editor for the Kluwer International Series on Biometrics, and an associate editor of several international journals, such as the *IEEE Transactions on Systems, Man, and Cybernetics* and *Pattern Recognition*. He has been a guest editor of special issues on biometrics in several journals, such as the *IEEE Transactions on Systems, Man, and Cybernetics-C* and *Pattern Recognition*, and chairman of the Hong Kong Biometric Authentication Society. His research interests include automated biometrics-based authentication, pattern recognition, biometric technology, and systems. As a principal investigator, he has finished many biometrics projects since 1980. So far, he has published more than 200 papers and seven books, including *Parallel Computer System Designs for Image Processing & Pattern Recognition* (HIT, 1998), *Parallel VLSI Neural System Design* (Springer, 1999), *Automated Biometrics: Technologies and Systems* (Kluwer Academic, 2000), *Data Management and Internet Computing for Image/Pattern Analysis* (Kluwer Academic, 2001), *Neural Networks and Systolic Arrays Design* (World Scientific, 2002), and *Biometrics Resolutions for Authentication in an e-World* (Kluwer Academic, 2002). He is a senior member of the IEEE and a member of the IEEE Computer Society.